ELSEVIER

Journal of Nuclear Materials 307–311 (2002) 393–397

journal of nuclear materials

www.elsevier.com/locate/jnucmat

Microstructural examination of irradiated and unirradiated V–4Cr–4Ti pressurized creep tubes

D.S. Gelles *

Pacific Northwest National Laboratory, MS P8-15, P.O. Box 999, Richland, WA 99352, USA

Abstract

Microstructures of three pressurized tubes of V–4Cr–4Ti heat 832665 following irradiation in the Advanced Test Reactor at ~300 °C to ~5 dpa are examined and compared with thermal creep tubes tested at 700 and 800 °C. Irradiation creep response at 300 °C is found to be associated with dislocation development and may be affected by precipitation. Stress appears to encourage grain boundary migration during irradiation creep. Segregation of Cr to boundaries and Si behind boundaries was found to accompany the grain boundary migration. Thermal creep is probably due to dislocation climb influenced by TiO_2 precipitation.

1. Introduction

Application of vanadium alloys such as V–4Cr–4Ti for fusion requires understanding of irradiation creep response in order to optimize reactor design. A number of experiments are underway in order to provide that data [1–4], but the nature of irradiation creep experiments limits the number of data points that can be accumulated. Generally, this is done by irradiating pressurized tubes and determining the change in tube diameter as a function of irradiation dose. However, recent experiments do not allow reirradiation of specimens and therefore a diameter change measurement includes effects of primary creep, steady state creep, and perhaps, tertiary creep, as well as effects of swelling and densification due to precipitation. It is therefore beneficial to characterize the microstructure and to measure densification and swelling response in order to better assess pressurized tube response. This report is intended to provide microstructural examinations of pressurized tubes of V–4Cr–4Ti heat 832 665 following irradiation in the Advanced Test Reactor, Idaho Falls, at ~300 °C to ~5 dpa in comparison with thermal response at 700 and 800 °C.

2. Experimental procedure

Details for the pressurized tubes examined in this study are provided in Table 1. Ring sections of tubing were sectioned and ultrasonically drilled or punched to produce 3 mm curved disks. Disks were thinned by grinding but evidence of the curvature was retained in order to be able to orient the microstructure relative to the stress state. Disks were then electropolished at low temperature (~−40 °C) in a 5% sulfuric acid–methanol solution at ~40 V using standard techniques to produce thin foils. Each disk was mounted in the microscope so that images could be related to the tube orientation and therefore the state of stress could be related to the microstructure (generally, the tube length parallel to the side-entry stage axis). Dislocation imaging involved procedures that allowed identification of all $(a/2)\langle 1\,1\,1\rangle$ Burgers vectors present [5].

3. Results

Specimens for TEM were successfully prepared from all specimens but for unirradiated conditions AR15, AR17 and AR19 thin area was limited. All unirradiated microstructures were found to contain a moderate density of dislocations non-uniformly distributed. However,

* Tel.: +1-509 376 3141; fax: +1-509 376 0418.
E-mail address: ds_gelles@pnl.gov (D.S. Gelles).

0022-3115/02/$ - see front matter
PII: S0022-3115(02)01007-3

Table 1
Conditions for specimens examined

ID	Hoop stress (MPa)	Temperature (°C)	Time to failure/dose	Strain (%)
AR15	159	700	2804 h	13.0
AR17	93	800	864 h	13.6
AR18	118	800	578 h	24.1
AR19	137	800	242 h	14.7
A1	0	286	4.3 dpa[a]	0.11
A10	87	302	4.6 dpa[a]	0.10
A7	129	300	4.7 dpa[a]	0.28

[a] 133 EFPD or 3192 h.

evidence for clearly defined cell walls and therefore a cell diameter characteristic of dislocation-controlled thermal creep behavior were not found. Instead the structure contained areas with higher or lower dislocation density, depending on location. However, in the vicinity of larger TiO_2 precipitate particles (~200 nm in diameter), the dislocation density was significantly higher, indicating that such particles were probably obstacles to dislocation evolution.

Examples of the unirradiated microstructures found are given first for specimens tested at 800 °C and then for the specimen tested at 700 °C. Fig. 1 shows low magnification examples of specimen AR17, tested at 800 °C. Fig. 1(a) and (c) provide examples of grain boundary nodes indicating that most grain boundaries are straight and precipitate free, but some are heavily decorated with precipitation, presumably formed on cooling during heat treatment [6]. Fig. 1(b) and (c) indicate that the dislocation structure consists of a moderate dislocation density, but 200 nm diameter precipitate particles may be decorated at higher density. Also, Fig. 1(b) shows evidence of a poorly defined cell structure towards the center of the micrograph.

Fig. 2 shows the dislocation structure in greater detail for specimens AR17 and AR19, respectively. The structures are shown using $\langle 1\,1\,0\rangle$ bright field images, so that only two of the four sets of $\langle a/2\rangle\langle 1\,1\,1\rangle$ dislocations can be seen. From these figures, several observations can be made. The dislocation structure is non-uniformly distributed, with highest density near large TiO_2 particles, but with formation of poorly defined cell walls, and containing lowest densities between these cell walls. However, many small dark features that formed during thermal creep exposure can be identified, believed to be precipitation of Ti(O,C,N) type based on behavior at higher and lower temperatures.

Finally, Fig. 3 is provided, showing examples of the dislocation structure found in specimen AR15, tested at 700 °C. In each case, contrast is due to $\langle 0\,1\,1\rangle$. Fig. 3 demonstrates that dislocation evolution during thermal creep at 700 °C is similar to that found at 800 °C.

The microstructure of the irradiated unstressed condition A1 is shown in Fig. 4. This figure and the one that

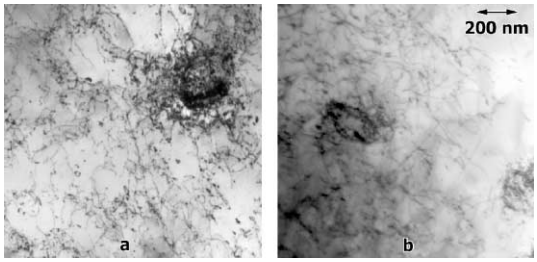

Fig. 2. Dislocation structures found in specimens AR17 and AR19 with $g = \langle 1\,1\,0\rangle$ vertical.

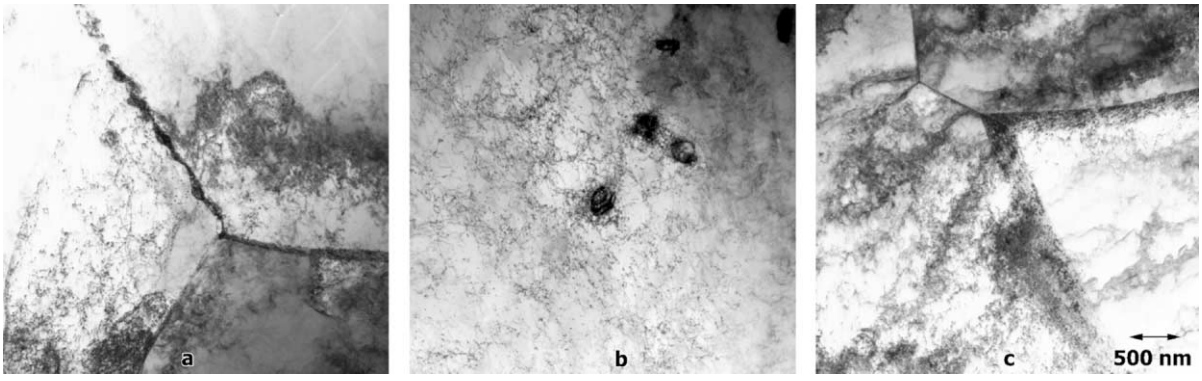

Fig. 1. Low magnification examples of the microstructure of specimen AR17.

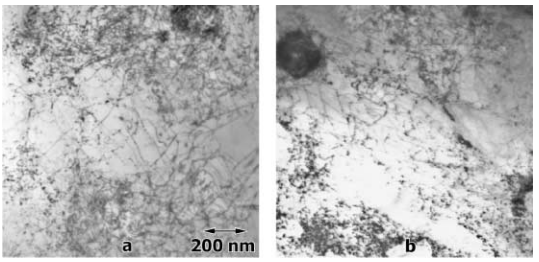

Fig. 3. Examples of dislocation structures found in specimen AR15.

follows have been prepared to allow identification of all $(a/2)\langle 1\,1\,1\rangle$ Burgers vectors present with images in $0\,1\,\bar{1}$ contrast and in 200 contrast taken near a $(0\,1\,1)$ orientation and the third in $\bar{1}\,0\,1$ contrast was taken after a large tilt of the foil. A large TiO_2 particle is located on the lower right in order to reveal any changes in behavior near such particles.

Similar images are also provided for the stressed condition A7 in Fig. 5. Examination and comparison of Figs. 4 and 5 reveals that dislocation images are difficult to identify due to extensive precipitation that is present. Similar response was found for condition A10. Diffraction only revealed additional intensity in the vicinity of $(2/3)\langle 2\,2\,2\rangle$. The dislocations appear to be only of type $(a/2)\langle 1\,1\,1\rangle$, based on imaging under 200 strain contrast, as is usually the case in vanadium alloys. No evidence for void swelling could be identified.

In the course of examination of condition A7, it became apparent that several examples of grain boundary migration could be identified. Two examples are provided in Fig. 6. In the first case, the boundary has moved

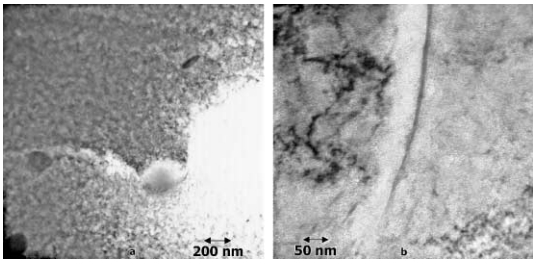

Fig. 6. Examples of grain boundary migration in condition A7 at 300 °C, 129 MPa to 4.3 dpa.

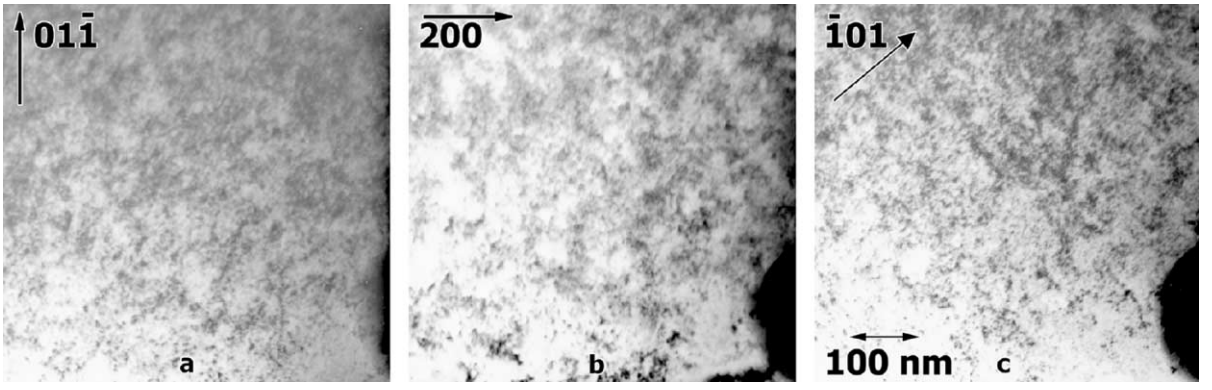

Fig. 4. Condition A1 at 300 °C, 0 MPa to 4.3 dpa and 0.11% strain.

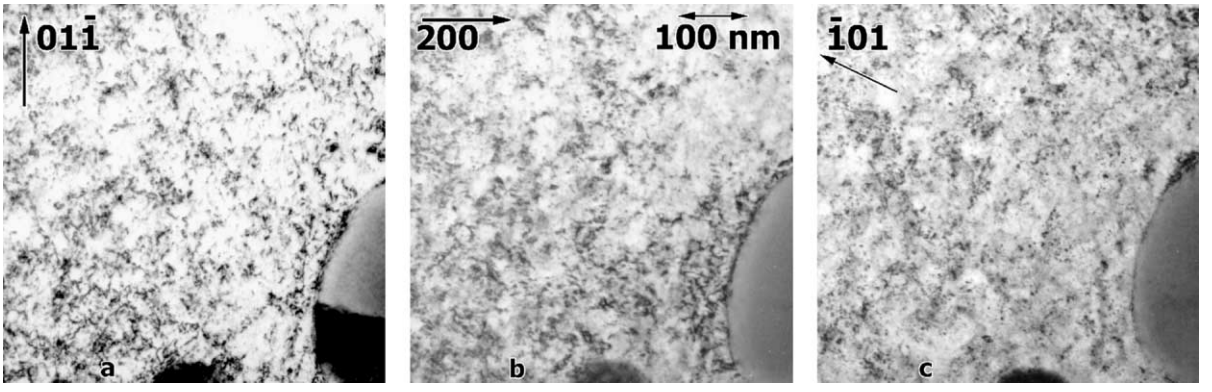

Fig. 5. Condition A7 at 300 °C, 129 MPa to 4.7 dpa and 0.28% strain.

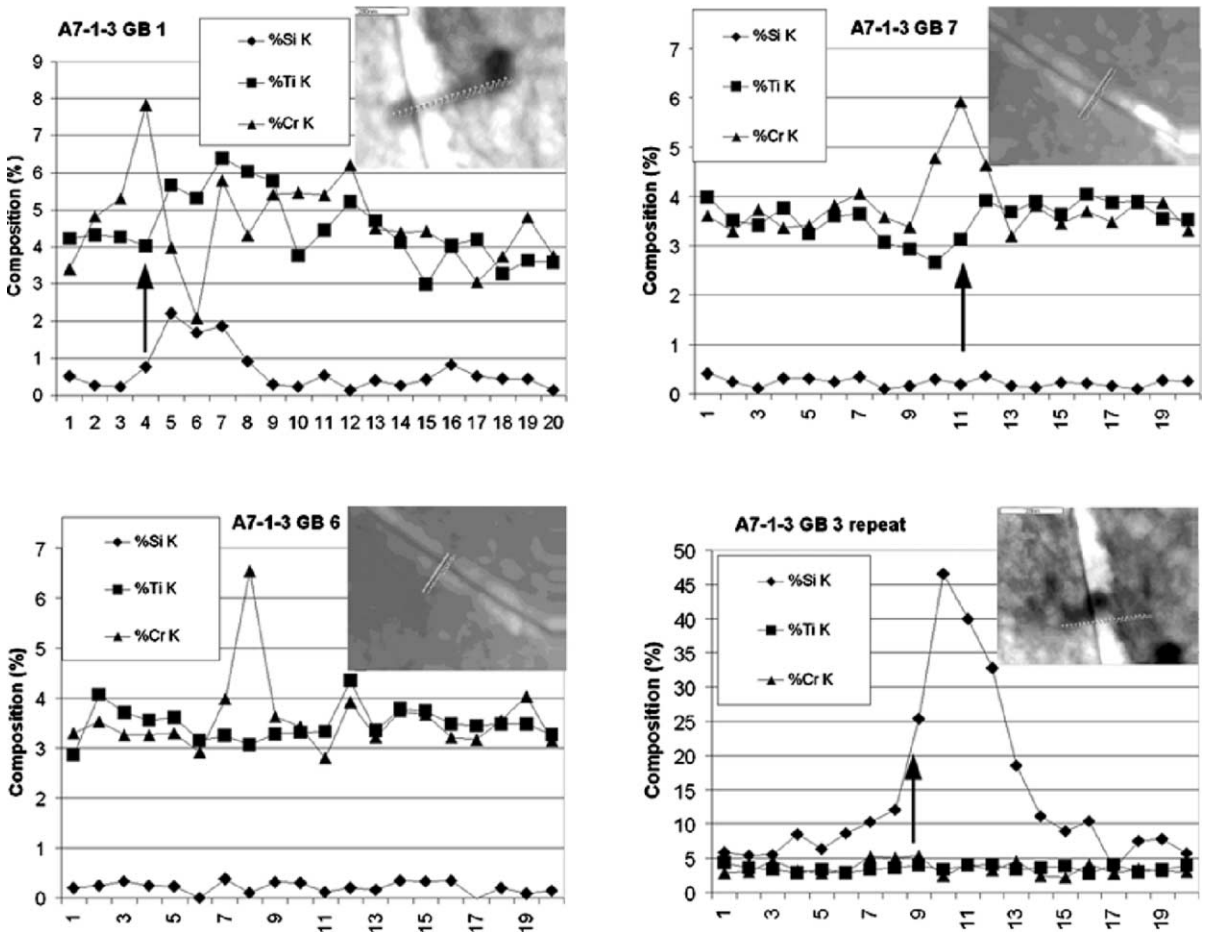

Fig. 7. Grain boundary composition profiles in condition A7 at 300 °C, 129 MPa to 4.3 dpa.

but was pinned by a large TiO_2 particle, so migration probably is on the order of 800 nm, or close to 1 μm, a large distance compared to the effective matrix diffusion distance for this irradiation temperature. In the second case, the boundary has polished differently than the surrounding matrix with what appears to be a denuded zone (without precipitation, perhaps) adjacent. Specimen A7 was further examined using field emission gun analytical electron microscopy in order to identify chemistry changes near migrating boundaries. Results are given in Fig. 7 showing plots of composition as a function of position across the boundary which is marked with an arrow. A digital image is inset for each plot in order to show the positions of the points analyzed. Scan 'gb 1' indicates enhancement of Cr at the boundary and depletion to the right with accompanying enhancement of Si behind the boundary. Scans 'gb 6' and 'gb 7' of the same boundary but at different locations confirm Cr enrichment at a boundary that probably did not migrate. Scan 'gb 3 repeat' demonstrates extremely high Si levels for another boundary that migrated. Therefore, enrichment due to Cr and Si is indicated, with the Si enrichment behind the migrating grain boundary, but Ti shows negligible evidence of enrichment.

4. Discussion

The microstructures found following thermal creep indicate that strain is controlled by dislocation climb. This is confirmed by the elongated grain structure found using optical microscopy [2] and in agreement with the high stress exponent found for other tests [1]. However, it is also apparent that large TiO_2 particles play a role in controlling creep rates by acting as obstacles to dislocation climb. And the consequences of the small features found following thermal creep and expected to be Ti(O,C,N) precipitation are not yet understood. The lack of a well-defined dislocation cell structure, and therefore, a well-defined cell size, is possibly a consequence of the lack of steady state creep response.

A concern with the microstructural observations is that specimen preparation procedures may have affected the observed dislocation structures. TEM specimen preparation using ultrasonic drilling has not been used in the past, but was warranted because of the variation in tube diameter found following creep testing. As control specimens were not prepared, it cannot be shown conclusively that ultrasonic preparation has not influenced the results. Also, although most dislocation images appear to be typical of climbing dislocations, Fig. 2(a) can be interpreted to contain a large number of slip dislocations oriented for optimum slip.

The results of microstructural examinations of irradiated V–4Cr–4Ti pressurized tubes may be summarized as follows: (1) extensive fine precipitation was found with diffraction intensity at $(2/3)\langle 2\,2\,2\rangle$. Precipitates may be nucleating near dislocation structure. (2) The dislocation structure consisted of perfect dislocation line segments with few loops identified. (3) Stress appears to encourage grain boundary migration. (4) Evidence for segregation of Cr to boundaries and Si behind boundaries was found to accompany grain boundary migration.

Therefore, irradiation creep of V–4Cr–4Ti is probably also controlled by climb of $(a/2)\langle 1\,1\,1\rangle$ dislocations. Grain boundary migration is observed, probably enhanced by stress, but it is not anticipated that grain boundary sliding plays an important role in deformation. As with unstressed conditions, precipitation at low temperatures is extensive, obscuring other microstructural features and probably leading to irradiation hardening. Identification of the precipitate remains poorly defined. No evidence for non-steady state creep could be found.

Finally, it should be noted that a companion paper included in this proceedings provides similar results for V–3Fe–4Ti–0.1Si, but did not show precipitation during low temperature irradiation [7], although interstitial oxygen and nitrogen levels were similar.

5. Conclusions

Failed V–4Cr–4Ti biaxial thermal creep specimens have been examined using OM, SEM and TEM in order to assess creep and failure mechanisms. It was found that deformation is probably due to dislocation climb, influenced by TiO_2 precipitation, and that lack of steady state creep response could be due to minor tube defects.

Irradiation creep at 300 °C is associated with dislocation development and may be affected by precipitation. Stress appears to encourage grain boundary migration during irradiation creep. Segregation of Cr to boundaries and Si behind boundaries was found to accompany the grain boundary migration.

Acknowledgements

This work would not have been possible without the cooperation and participation of H. Tsai and coworkers at the Argonne National Laboratory. Pacific Northwest National Laboratory (PNNL) is operated by the US Department of Energy by Battelle Memorial Institute under contract DE-AC06-76RLO-1830.

References

[1] R.J. Kurtz, M.L. Hamilton, DOE/ER-0313/25 (1999) 7.
[2] D.S. Gelles, M.L. Hamilton, R.J. Kurtz, DOE/ER-0313/26 (1999) 11.
[3] H. Tsai, H. Matsui, M.C. Billone, R.V. Strain, D.L. Smith, J. Nucl. Mater. 258–263 (1998) 1471.
[4] H. Tsai, M.C. Billone, R.V. Strain, D.L. Smith, DOE/ER-0313/23 (1998) 149.
[5] D.S. Gelles, A. Kimura, R.J. Puigh, DOE/ER-0313/12 (1992) 123.
[6] D.S. Gelles, H. Li, DOE/ER-0313/19 (1995) 22.
[7] K. Fukumoto, S. Takahashi, R.J. Kurtz, D.L. Smith, H. Matsui, these Proceedings.